Title page

Names of the authors: Eros Mossini, Luca Codispoti, Giorgio Parma, Filippo Maria Rossi, Elena Macerata, Alessandro Porta, Fabrizio Campi, Mario Mariani

Title: MCNP model of L-54 M nuclear research reactor: validation by preliminary graphite radiological characterization

Affiliation(s) and address(es) of the author(s): Department of Energy, Politecnico di Milano, Piazza L. da Vinci 32, I-20133 Milano, Italy

E-mail address of the corresponding author: eros.mossini@polimi.it;
lucasaverio.codispoti@polimi.it

MCNP model of L-54 M nuclear research reactor: validation by preliminary graphite radiological characterization

Eros Mossini Correspondent[1], Luca Codispoti[1], Giorgio Parma[1], Filippo Maria Rossi[1], Elena Macerata[1], Alessandro Porta[1], Fabrizio Campi[1], Mario Mariani[1] Co-Authors

[1] *Department of Energy, Politecnico di Milano, Piazza L. da Vinci 32, I-20133 Milano, Italy*

Abstract

Since its shutdown in 1979, L-54M nuclear research reactor of Politecnico di Milano has been kept in safe storage configuration. In view of forthcoming decommissioning activities, many characterization activities have been performed on its matrices. Regarding the L-54M graphite stack, a neutron activation model was developed and validated by a graphite sampling and preliminary radiological characterization campaign focused on the most significant gamma-emitting radionuclides.

Even if slightly underestimating the measured values, between -5% and -49% for ^{152}Eu, between -41% and -67% for ^{154}Eu, the simulated activity concentrations promisingly reproduce the experimental radial profile.

Keywords

Decommissioning, Radiological Characterization, AGOT Graphite, Neutron Activation, MCNP neutronic model, Gamma Spectrometry (HPGe)

Introduction

Commissioned to Atomics International in late ’50 and built on CeSNEF (*Centro Studi Nucleari Enrico Fermi*) site in 1958, L-54M is the thermal nuclear research reactor (50 kW_{th} nominal power) of Politecnico di Milano that was used for conducting a variety of scientific studies and experimental works on nuclear reactor physics, radiochemistry, materials irradiation, radiation detection and measurement [1] [2].

Its core is a sphere made of nuclear grade stainless steel filled with a liquid uranyl sulfate fuel solution enriched up to 19.94 %wt in ^{235}U. The water-based fuel solution was an efficient primary source of moderation for the neutron flux. The neutron moderation and reflection were also assisted by a stack of nuclear grade Atcheson Graphite Ordinary Temperature placed all around the core. The biological shield, made of heavyweight magnetite–colemanite concrete, surrounds the whole critical structure in order to reduce the radiation emission to the workplace coming from the core. This nuclear pile achieved its first criticality condition in 1959.

L-54M worked discontinuously and rarely at its nominal power for 20 years as long as it was shut-down in 1979. After a routine reactor downtime, the Italian Nuclear Safety Competent Authority did not renew the authorization to restart the activities as a consequence of the growth of a highly-populated urban area around the nuclear site at that time [3] [4]. Once that this status was officially assumed as permanent, Politecnico di Milano developed a dismantling plan for L-54M research reactor. Worldwide, three are the main decommissioning strategies that have been adopted so far depending on political, economical, technological and social contingencies: 1) immediate dismantling, when the final phase starts exactly after the plant shutdown; 2) safe enclosure, in which the facility is placed and maintained in a safe long term condition until decontamination and dismantling actions are launched; 3) entombment, when the activated and contaminated structure, systems and components of the nuclear plant are covered and shielded in a long-term stable structure [5] [6].

During the ’80s, the lack of a radioactive waste national repository led all the Italian owners of the permanently shut-down nuclear installations to choose the safe enclosure option as the only feasible strategy. This approach allows to reduce the level of radioactivity due to short-living radionuclides before the dismantling operations begin and offers a useful delay to collect the required funds for the safe decommissioning

program implementation. Furthermore, the deferred dismantling strategy requires minimal personnel, plant maintenance actions and regulatory controls in view of guaranteeing safety of nuclear facility, public and environment [7] [8].

The transition period occurs between plant operation and safe enclosure or dismantling status and is focused on guaranteeing a safe and stable condition of the facility [9]. During that period, Politecnico di Milano carried out several transition activities as the spent nuclear fuel solution removal from the plant and its shipment to a reprocessing facility, the Ra-Be neutron start-up source extraction from the graphite stack, the primary circuit decontamination and the radiological pre-characterization of L-54M CeSNEF Structures, Systems, Components and site. These activities were aimed at obtaining the radiological map of the plant and the evaluation of the radioactive waste volume that the forthcoming decommissioning activities would produce [10] [11] [12]. At the end of 2016, Politecnico di Milano joined IAEA collaborative research project on irradiated GRAphite Processing Approaches (GRAPA) that is focused on defining safe and feasible industrial waste management processes for the irradiated graphite [13]. In order to support the radiological characterization of L-54 M moderator and reflector graphite, a neutronic model of the reactor has already been developed by MCNP (Monte Carl N-Particle) [7] [14] [15] [16]. This probabilistic Monte Carlo code was chosen for the simulation considering its well documented capabilities for this task, as it can be found in the literature [17] [18]. Furthermore, this computational approach is recommended for the radiological characterization of radioactive matrices, when neutron activation prevails on contamination [17]. As a result, this method allowed to determine the activity concentration of the most relevant radionuclides in the whole graphite stack. The model development and its preliminary verification have already been presented in previous publications [14] [15] on the basis of experimental criticality and fluences data.

This paper aims at presenting a briefly overview of the sampling characterization campaign of L-54M irradiated graphite stack and the relative experimental gamma spectrometry measurements with the scope of validating the formerly developed neutron activation model. For this purpose, several samples were collected at different axial and radial positions with respect to the core from the accessible parts of the graphite structure, in particular from its west surface and along the length of two extractable rods on the east

access. In this paper, the comparison between the experimentally measured activity concentrations of the most relevant gamma-emitting radionuclides (^{152,154}Eu, ^{133}Ba and ^{137}Cs), determined by High Purity Germanium (HPGe) gamma-spectrometry, and the simulated values, obtained with the Monte Carlo code, is presented. This whole work aims at highlighting the strength and the accuracy of the computational approach in supporting pre-decommissioning radiological characterization campaigns.

Experimental

Sampling and sample preparation

In order to confirm the 3D activation model outcomes developed by the MCNP6 code, Politecnico di Milano launched a new experimental radiological characterization campaign in January 2018. Several points had been identified as relevant on two accessible parts of the graphite stack: 7 samples were picked-up from the western surface of the stack (*top*) and other 10 along two (Top, Bottom) east side removable rods (*center* and *bottom*) of the at different axial and radial positions with respect to the core.

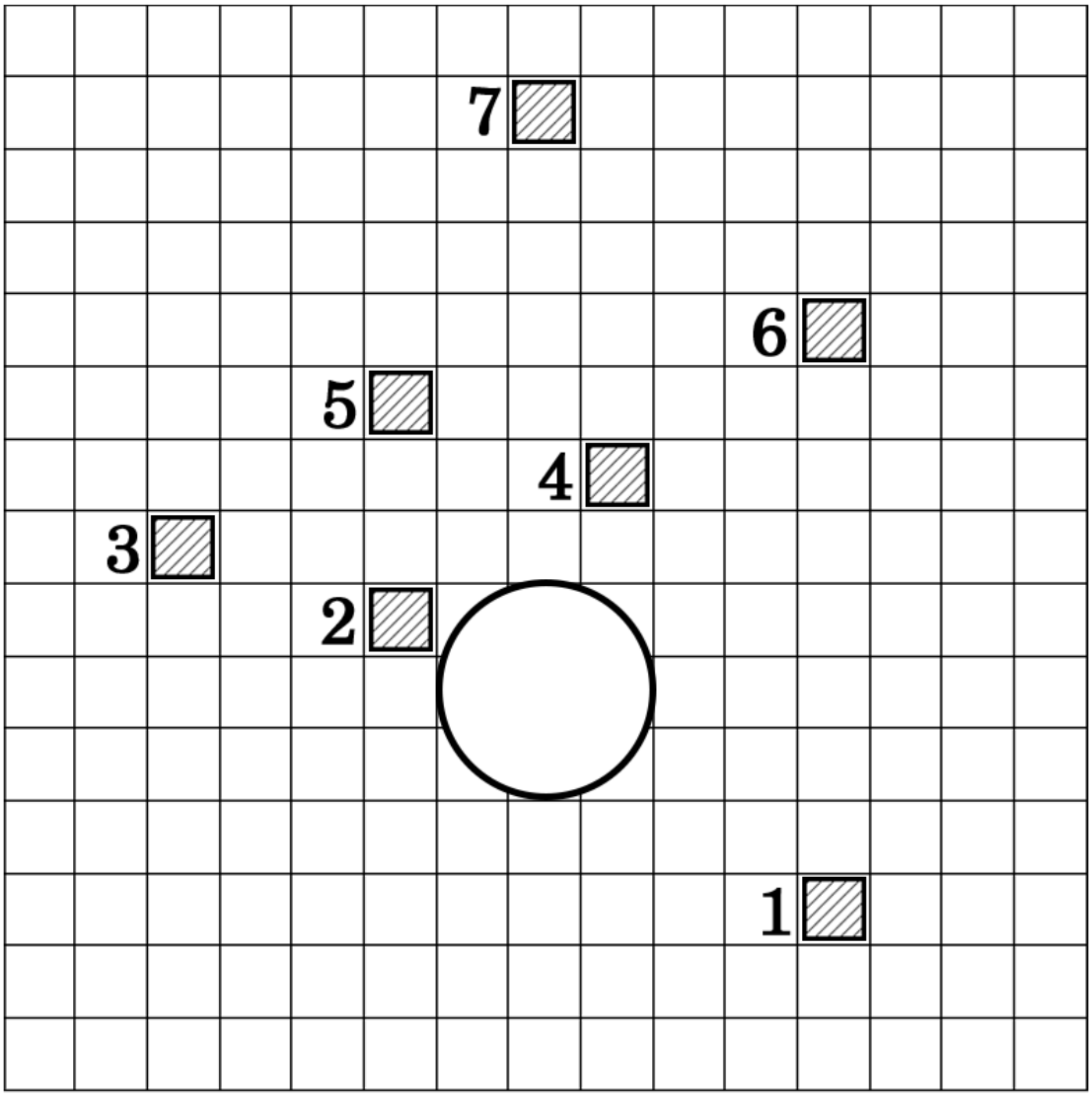
7
6
5
4
3
2
1

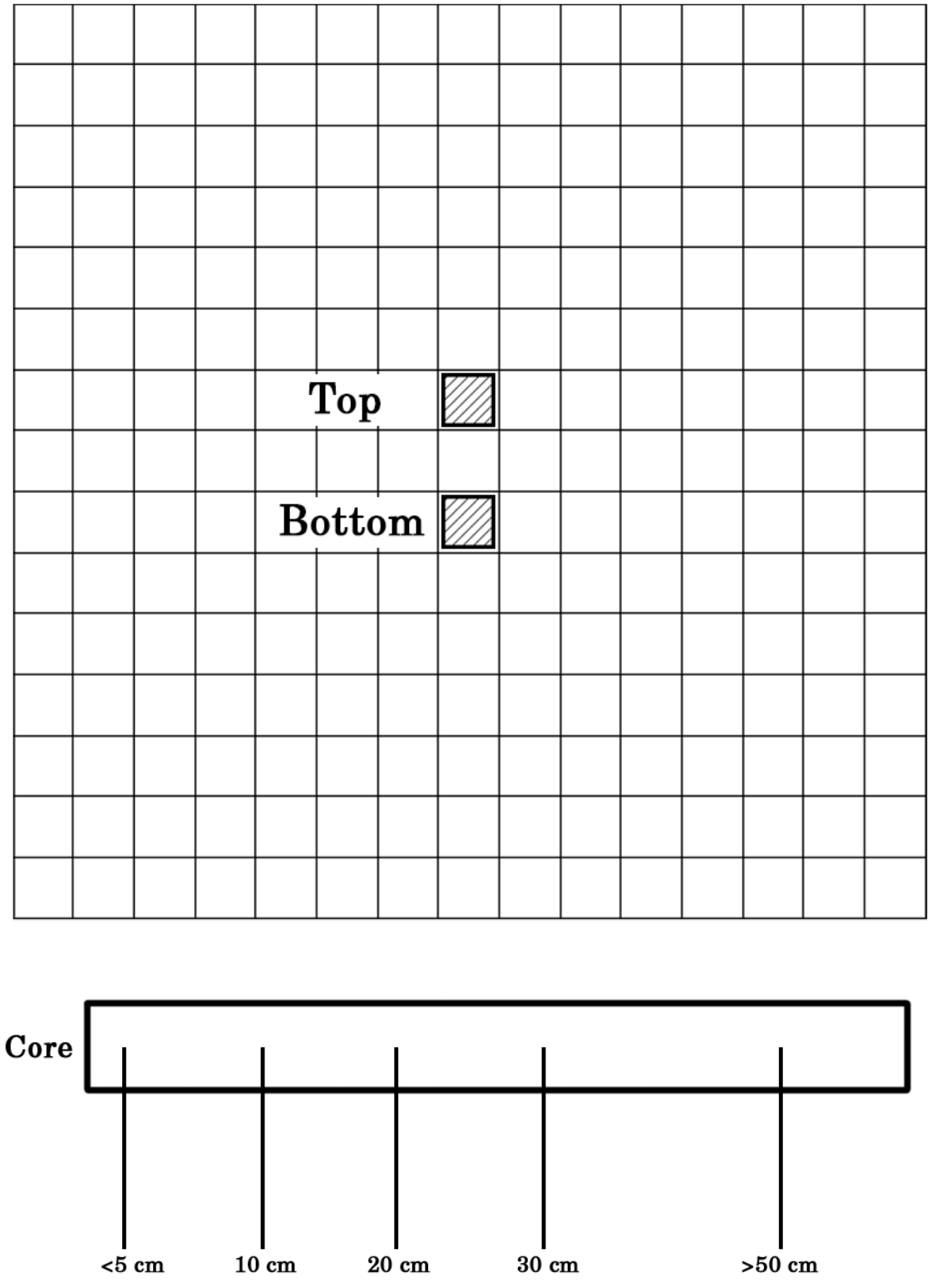

108

Figure 1 Location of the collected irradiated graphite samples on the west surface (*top*) and on the two east surface rods (*center, bottom*) [14] [15]

The sampling activities took place in the Reactor Hall, inside an operative area continuously kept in a negative pressure status also during the L-54M CeSNEF Safe Enclosure Condition: the primary air pipes system continuously supplies ventilation in the Reactor Building with the exit pipe lines connected to absolute particulate HEPA filters (ε = 99.98%; d= 0.3 μm).

In order to avoid the potential dispersion of any radioactive dust during samples collection, every phase or action was performed in a dynamic confinement system made by technical tents of high density polyethylene (HDPE) already installed on the two accessible irradiated graphite stack entrances (West side, East side). In order to ensure a sufficient air exchange in each tent (*i.e.* 5 times per hour), a forced ventilation system was connected to absolute particulate HEPA filters (ε = 99.98%; d= 0.3 μm) and put in operation. A SAS (Safety Access System) entrance was also predisposed in order to create a decontamination buffer zone for the operating staff, the instrumentations and the sampling tools (Figure 2).

Figure 2 HDPE tent and extracted irradiated graphite rod before sampling.

Based on these collective and environmental protective devices and on the radiation protection principles, Politecnico di Milano Radiation Protection Expert predisposed an operational safety program of the sampling activities. In order to identify the best procedures and equipment, a preliminary professional dose assessment on external

exposure and on potential internal contamination was performed upon the technical team involved in the work [19] [20], also depending on their specific tasks:

a) Supervisor – the team manager directly involved in the sampling activities inside the technical tents

b) Technical Operator – the team member specialized in radiological measurements and in collecting samples; he was authorized to enter the technical tents.

c) Health Physics Operator – the team member specialized in radiological measurements and decontamination actions on active workers; he was authorized to enter the technical tents just in case of accidents or emergencies.

Each of them worn dedicated disposable protective clothing as integral Tyvek® suit, cotton and nitrile gloves, Tyvek® overshoes, P3 absolute filter global masks during the L-54M irradiated graphite stack samplings operations. The Ambient Dose Equivalent Rate ($\dot{H}^*$ (10)) in the Reactor Hall, the Personal Dose Equivalent Rate ($\dot{H}$p(10)) and the removable surface contamination were continuously monitored during activities using active portable devices (in-line monitoring): the maximum dose rate value measured in the Reactor Hall, with removable reactor doors closed, was below 0.5 µSv h^{-1}; in the working area, with removable reactor door opened, the dose rate value was close to 3 µSv h^{-1}.

With a view to experimentally estimating the professional effective dose during the sampling campaign, suitable electronic dosimeters were employed and ^{14}C, ^{3}H, ^{152}Eu analyses were performed using active air samplers filters placed inside the technical tents. Nasal swabs were also carried out on operators in order to verify that no inhalation intake occurred [21].

Furthermore, at the end of the sampling phase, several smear tests were performed aiming at excluding the potential environmental contamination of the surfaces (buffer zones, technical tents) and of the devices after the sampling activities.

The Supervisor and the Technical Operator drilled seven irradiated graphite samples on the west side of the stack and other ten samples along the length of two east side extractable graphite rods at different axial and radial position with respect to the core. Right after drilling, the technicians poured the 17 irradiated graphite powder sample

(range weight: 15.7 – 28.4 g) in 250 ml plastic cylindrical beakers, sealed individually in PVC small transparent bags (Figure 3). A cylindrical sample holder had been evaluated as good compromise between capability and efficiency of HPGe gamma spectrometry measurements. Aiming at avoiding any potential cross-contamination, this samples configuration also allows a feasible transportation to Politecnico di Milano new integrated nuclear laboratories for the activity concentration analyses of the most relevant radionuclides.

Figure 3 Irradiated graphite powder sample in a 250 mL cylindrical beaker for γ-spectrometry

Gamma spectrometry measurement

To confirm the outcomes of MCNP activation code, in this preliminary analysis ^{152,154}Eu ^{133}Ba, ^{137}Cs activity concentrations were measured by in-Lab HPGe γ-spectrometry. An initial qualitative identification of these most relevant radionuclides present in L-54M irradiated graphite was performed using a P-type coaxial HPGe (ORTEC GEM model) detector. As shown in Table 1, selected gamma full energy peaks were identified for a more efficient and reliable quantitative assessment [22].

Table 1 Selected full energy peaks of the gamma-emitting radionuclides, expressed in keV and their mean real efficiency

Radionuclide	Energy [keV]	Mean Real Efficiency
^{152}Eu	778.9 1408.01	2.25E-02 ± 7.49E-05 1.54E-02 ± 6.22E-05
^{154}Eu	1274.4	1.67E-02 ± 8.01E-05
^{133}Ba	302.85 356.01	5.29E-02 ± 1.42E-04 4.64E-02 ± 1.09E-04

Due to its high-performance semiconductor properties, this P-type coaxial detector is designed to offer a high-quality energy resolution (FWHM = 1.85 keV at 1.33 MeV peak of ^{60}Co) and is set to cover a wide gamma energy range (40 keV upward). Internally surrounded by cadmium and copper layers (1.2 mm and 1 mm), a shield of lead (10 cm thickness) is placed around the GEM capsule to reduce the background noise.

Managing the spectrum information recorded in the multichannel analyzer, GammaVision MCA emulation software was utilized to identify the gamma full energy peaks net counts. In particular, the software is endowed with basic (energy calibration, background subtraction, peak identification) and advanced (gaussian interpolation peak) application tools for the gamma analysis. Once the specific gamma radionuclides library is defined, the samples radiological blank (c_B) and the total (c_S) counts were achieved for each region of interest (ROI). [23] An empty cylindrical holder is the radiological blank and it is measured for 81000 s in the same configuration of the samples.

The ratio between the recorded pulses and all the gamma particles emitted from the measured radioactive sample is defined as detector absolute efficiency (ε). Depending on the physical parameters of matrices and on those of the HPGe detector, an experimental evaluation of the efficiency can be complex, especially due to the matrix self-attenuation and the gamma lines coincidence-summing effects. Considering the detector and shield specifications (provided by the vendor), the measuring geometric configuration and the sample density and composition, a semi-Monte Carlo simulation software was employed to simulate the interaction between the emitted gamma photons, the sample and the

detector. The computational code used in this work for evaluating the peak efficiency of each selected full energy peak was GESPECOR. The so-obtained efficiency calibration curve for the irradiated graphite samples is reported in **Table 1Errore. L'origine riferimento non è stata trovata.** [24].

The activity concentration of the selected gamma emitting radionuclides was achieved according to the Eq. 1:

$$A[Bq\ g^{-1}] = \frac{\frac{c_S}{T_S} - \frac{c_B}{T_B}}{BR\ m\ \varepsilon} \quad \text{Eq. 1}$$

where:

- c_S and c_B are the counts of the sample and of the blank respectively
- T_S and T_B are the counting live times of the sample and of the blank (81000 s both)
- *BR* is the branching ratio of the specific gamma line
- *m* is the irradiated graphite powder sample mass in the cylindrical beaker
- ε is the detection efficiency of the gamma line calculated by the GESPECOR software

Minimum Detectable Activity concentration (MDAc) is used in the sample single hypothesis testing to verify if the measured activity concentration offers the appropriate level of statistical confidence with respect to the background. The statistical test is passed only if the measured activity concentration is greater than the MDAc, otherwise the measured data is not acceptable. MDAc was calculated according to Eq. 2:

$$MDAc[Bq\ g^{-1}] = \frac{L_D}{BR \cdot m \cdot \varepsilon} \quad \text{Eq. 2}$$

where: L_D is the Detection Limit and it was calculated according to Eq. 3 [25]:

$$L_D[cps] = \frac{3.29}{Tc} \cdot \sqrt{C_B \cdot \left(1 + \frac{T_c}{T_B}\right)} \quad \text{Eq. 3}$$

Simulation of activation by MCNP

Monte Carlo based codes have been widely recommended and exploited to simulate neutron activation of nuclear reactors components [17] [26] [18]. In this work, MCNP6 (Monte Carlo N-Particle, version 6) software package was chosen for its well-established performance and reliability concerning neutron diffusion and activation reaction studies [27]. The reactor was proficiently modeled up to the outer boundary of the heavyweight concrete biological shield by retrieving detailed geometrical and composition information from security and safety reports, blueprints and official documents [28] [2] [1] [29] [30].

A simplified sketch of the approach is reported in Figure 4.

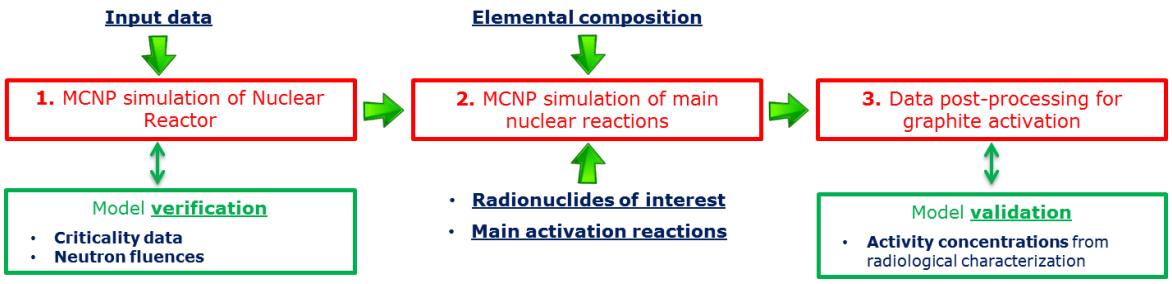

Figure 4 Sketch of the pursued computational approach.

The first step is dedicated to neutronic model implementation and verification with experimental criticality and fluences data. It has already been accomplished [14] [15]. As elsewhere described, all structural components were implemented in dedicated input sections, namely: cell, surface and material cards [15]. Several preliminary debugging experiments were carried out to identify potential mistakes. In order to ascertain if input data uncertainties affect model outcomes, a sensitivity analysis was performed. Moreover, experimental analyses were conducted to bridge some knowledge gaps, especially to accurately define macro constituents and impurities and better simulate neutrons diffusion and activation [14]. Given the unavoidable knowledge gaps and code implementation issues, the accuracy of the implemented model was satisfactorily verified by comparing several simulated criticality data (subcritical and supercritical reactivities, control rods total worth, inventory and calibration) and neutron fluxes in different core positions with the available experimental values [14] [15]. In order to calculate the

neutron multiplication factor, the criticality calculations were performed at ambient temperature (20°C) using *KCODE* card, a suitable number of cycles and neutrons/cycle. Moreover, simulations at the real reactor working conditions were conducted using the *TMP* card, the *makxsf* utility code and proper molecular scattering cross-sections datasets. The neutron fluences (expressed in cm^{-2}) were obtained with *F2* and *F4* tallies and processed as elsewhere described to obtain the most common flux formulations (expressed in n cm^{-2} J^{-1} or n cm^{-2} s^{-1}) [15]. In order to gather detailed activation maps of irradiated graphite, these calculations were performed on a dense mesh (1 cm^3 single element volumes) covering the whole graphite stack.

The second step (see Figure 4) is aimed at simulating the main activation reactions. It has already been described and partially accomplished in previous works [14] [15]. According to similar publications about irradiated graphite and coherently with time elapsed from reactor shut-down, these activation products were chosen: ^{3}H, ^{14}C, ^{36}Cl, ^{41}Ca, ^{55}Fe, ^{59}Ni, ^{60}Co, ^{63}Ni, ^{93}Mo, ^{94}Nb, ^{99}Tc, ^{108m}Ag, $^{152,154}Eu$, ^{233}U and ^{239}Pu. [18]. Accordingly, the main neutron activation reactions were chosen to identify the respective activation precursors (see Table 2). The precursors concentration in virgin materials was retrieved, either from available information or from new experimental campaigns. Afterwards, the reaction rates were calculated for each reaction and for all single element volumes, considering the precursor nuclide density, the respective activation reaction cross-sections and neutron flux [14] [15]. Moreover, the fission reactions on $^{235,238}U$ and ^{232}Th impurities were studied.

Table 2 List of radionuclides of interest and activation reactions.

Nuclide	$T_{1/2}$ (y)	Reactions
^{3}H	12.3	^{6}Li (n,γ) ^{3}H
		^{7}Li (n,α n) ^{3}H
		^{10}B (n,2α) ^{3}H
^{14}C	5730	^{13}C (n,γ) ^{14}C
		^{14}N (n,p) ^{14}C
^{59}Ni	7.6E+4	^{58}Ni (n,γ) ^{59}Ni
		^{60}Ni (n,2n) ^{59}Ni
^{63}Ni	100	^{63}Cu (n,p) ^{63}Ni
		^{62}Ni (n,γ) ^{63}Ni
^{93}Mo	4000	^{92}Mo (n,γ) ^{93}Mo

^{36}Cl	3E+5	^{35}Cl (n,γ) ^{36}Cl
		^{39}K (n,α) ^{36}Cl
		^{40}Ca (n,p) ^{36}Cl
^{41}Ca	1E+5	^{40}Ca (n,γ) ^{41}Ca
^{55}Fe	2.7	^{54}Fe (n,γ) ^{55}Fe
		^{56}Fe (n,2n) ^{55}Fe
^{60}Co	5.3	^{59}Co (n,γ) ^{60}Co

^{94}Nb	2E+4	^{93}Nb (n,γ) ^{94}Nb
^{99}Tc	2.1E+5	^{98}Mo (n,γ) ^{99}Mo
^{108m}Ag	418	^{107}Ag (n,γ) ^{108m}Ag
^{152}Eu	13.5	^{151}Eu (n,γ) ^{152}Eu
^{154}Eu	8.59	^{153}Eu (n,γ) ^{154}Eu
^{233}U	1.6E+5	^{232}Th (n,γ) ^{233}Th
^{239}Pu	2.4E+4	^{238}U(n,γ) ^{239}U

The purpose of the last step (see Figure 4) is to calculate, from the reaction rates, the activity concentration distribution of all the radionuclides of interest, as elsewhere described [14] [15]. Since the model validation relies on the comparison between calculated and experimental activity concentrations, the simulated data must be adjourned to the radiometric measure date. In this paper, just the gamma-emitting radionuclides (*i.e.* ^{152}Eu and ^{154}Eu) are considered for their usually lower uncertainty and easier sample preparation. Since the activity concentrations are simulated on a superimposed fine mesh (cubes of 1 cm^3), these data are properly averaged on several single element volumes to allow a direct and reliable comparison with the corresponding experimental samples.

Results and discussion

Gamma spectrometry results

The results of the radiological characterization along the length of the bottom (blue dots) and top (orange squares) irradiated graphite rods are plotted in Figure 5. The values trend reflects the activity concentration pattern of the most relevant L-54M irradiated graphite key radionuclides (^{152,154}Eu ^{133}Ba), in line with the L-54M neutron flux shape. The measured ^{137}Cs activity concentration values are below the respective MDAc.

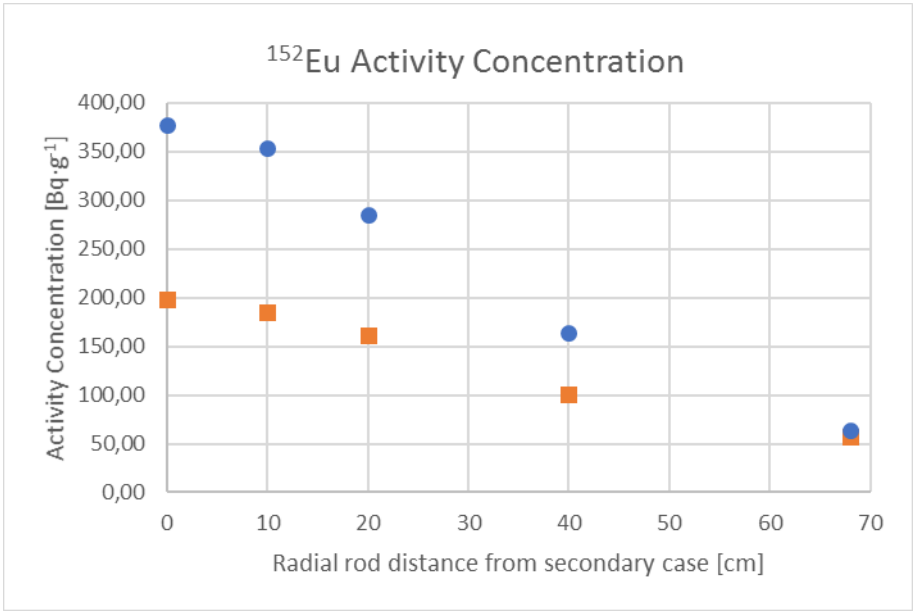
^{152}Eu Activity Concentration
Activity Concentration [Bq·g^{-1}]
400,00
350,00
300,00
250,00
200,00
150,00
100,00
50,00
0,00
0
10
20
30
40
50
60
70
Radial rod distance from secondary case [cm]

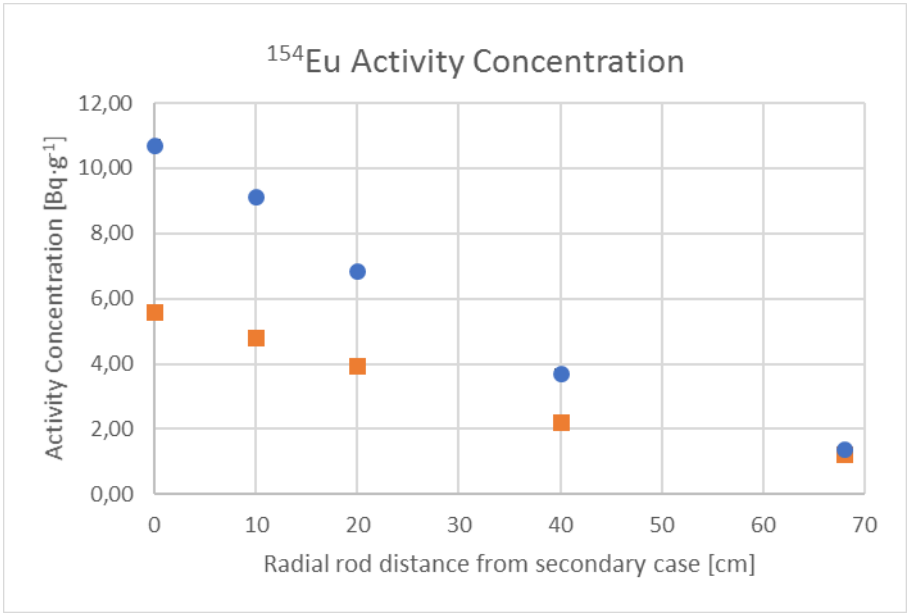
^{154}Eu Activity Concentration
Activity Concentration [Bq·g^{-1}]
12,00
10,00
8,00
6,00
4,00
2,00
0,00
0
10
20
30
40
50
60
70
Radial rod distance from secondary case [cm]

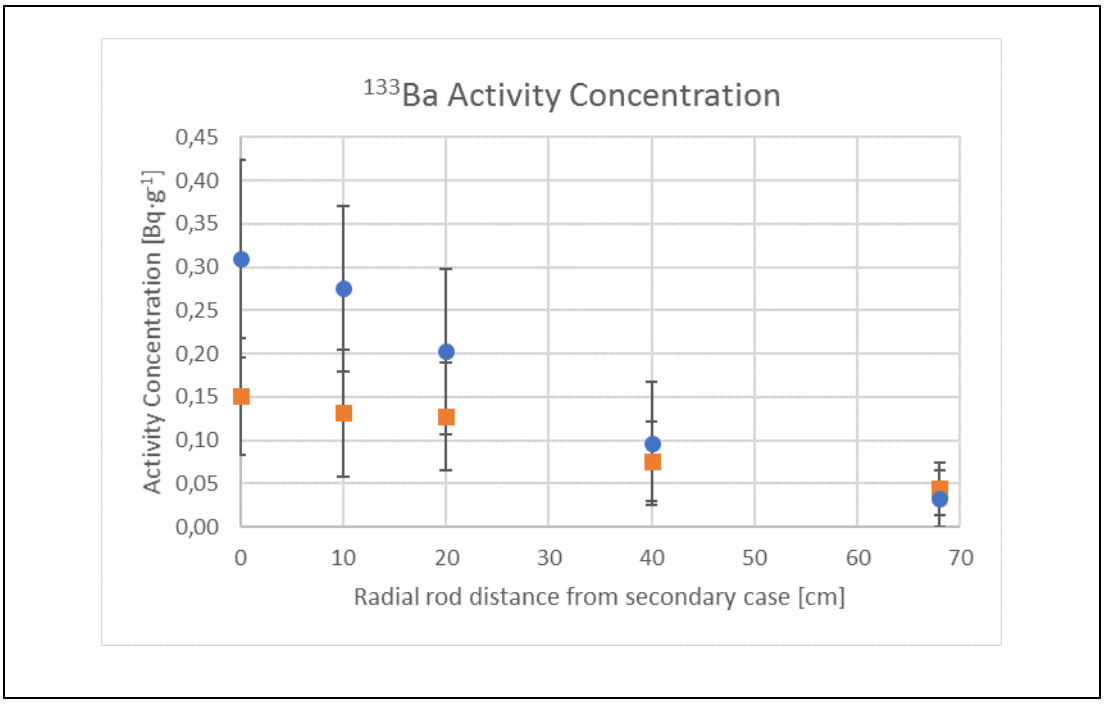

Figure 5 Activity Concentration Gradients of ^{152,154}Eu and ^{133}Ba comparing the two graphite rods. In case of ^{152,154}Eu, the error bars are within the marker size.

For the same radionuclides set, Table 3 offers the activity concentrations range and the related mean MDAc values in the 7 samples drilled on the accessible west surface of the graphite stack.

Table 3 Activity Concentration range and MDAc of ^{152,154}Eu, ^{133}Ba in the irradiated graphite

	Activity Conc. – Min [Bq g^{-1}]	**Activity Conc. – Max [Bq g^{-1}]**	**Mean MDAc [Bq g^{-1}]**
^{152}Eu	6.61 ± 0.13	79.59 ± 0.51	1.44E-02
^{154}Eu	0.16 ± 0.02	1.76 ± 0.05	7.16E-02
^{133}Ba	0.01 ± 0.01	0.07 ± 0.06	6.23E-02

In all the measured irradiated graphite samples, ^{137}Cs activity concentration values are below the respective MDAc ($2.3 – 4.1x10^{-3}$ Bq g^{-1}), thus they are not reported.

From the $^{152,154}Eu$ and ^{133}Ba highest activity concentration values found in sample #13 (Bottom rod – sample close to core), in sample #8 (Top rod – sample close to core) and in sample #4 (surface), the elemental distribution of L-54M virgin graphite can be roughly proved and assumed as homogeneous according to the following **Table 4**. Herein, the ratio between the activity concentration of minor gamma emitters (^{154}Eu and ^{133}Ba) and ^{152}Eu had been calculated and compared.

Table 4 Gamma emitting radionuclides percentage values in irradiated graphite samples

	Sample #13 - %	**Sample #8 - %**	**Sample #4 - %**
^{154}Eu	2.82 ± 0.05	2.81 ± 0.07	2.21 ± 0.07
^{133}Ba	0.08 ± 0.031	0.08 ± 0.034	0.08 ± 0.074

These outcomes show the graphite stack as an elemental homogeneous batch whose activation gradient is strongly dependent on the radial neutron flux shape.

MCNP results

The development of L-54M reactor neutronic model has already been satisfactorily achieved, even if some knowledge gaps could not be overcome [15]. As well, the simulated criticality and neutron fluence data within the core have already been satisfactorily compared with the available experimental ones [14]. The evidenced differences were explained by unavoidable lack of information and accuracy of some input data [1]. These results demonstrate that a reliable source characterization has been achieved by the implemented model. In order to complete this preliminary study, the verification of deep neutron transport from source to structural components has to be achieved by comparing simulated and experimental neutron fluxes in different materials. Unfortunately, just few experimental data concerning the exposure tubes crossing the core and the graphite moderator and reflector are available. In Figure 6, the simulated thermal flux in the exposure tube crossing the core is compared with the available

experimental data provided by the vendor [28] and by a M.Sc. thesis [30]. In particular, the irradiation channel crosses the core and the graphite reflector below and above 20 cm of radial distance, respectively.

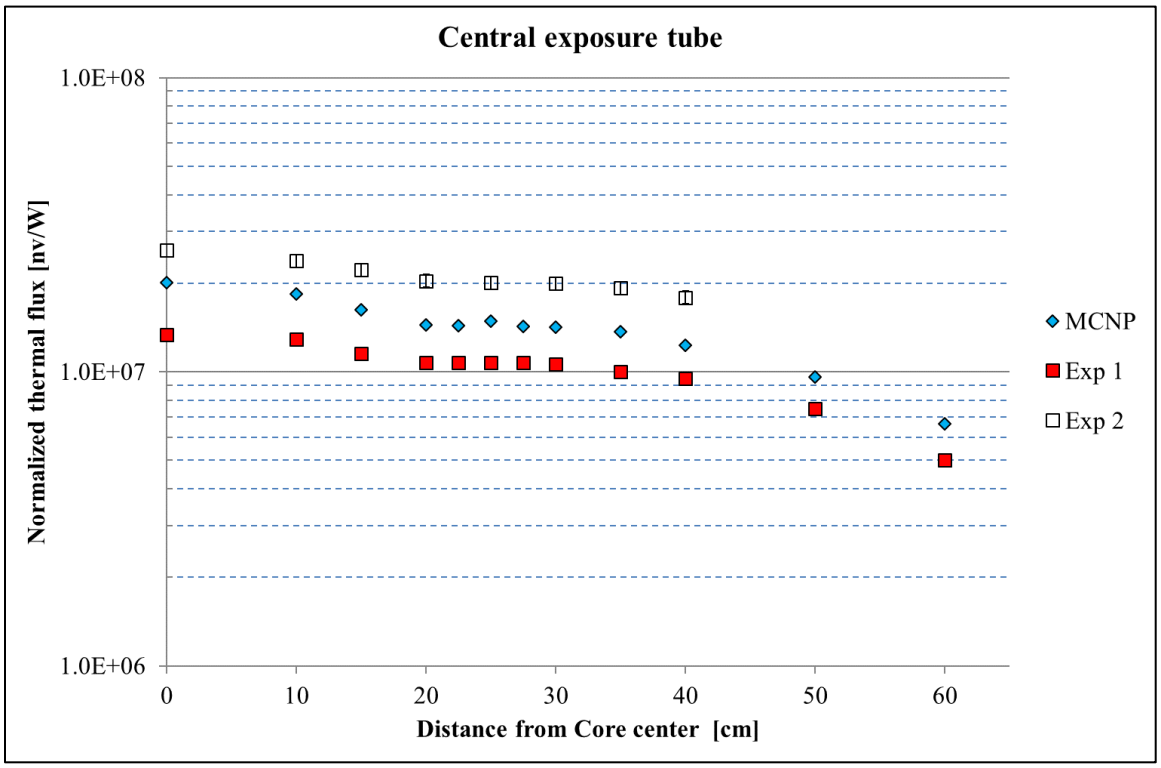

Figure 6 Normalized thermal flux in the central exposure tube as a function of radial distance from the core. *MCNP* (blue diamond, this work), *Exp 1* (red square, experimental data from **[28]**), *Exp 2* (empty square, experimental data from **[30]**). *Exp 1* data are provided without uncertainty. MCNP error bars are within the marker size.

As observable, the simulated flux values are of the same order of magnitude of the available experimental data sets. Furthermore, the same profile with the radial distance is evidenced, thus further proving that the developed neutronic model satisfactorily describes the main system physical properties. Similarly, the simulated thermal flux of other exposure tubes crossing the reflector graphite and the biological shield are compared with the experimental data provided by the vendor [28]. In Figure 7 and in Figure 8 the calculated and experimental thermal fluxes of exposure tubes 4 and 8 are reported. In both cases, the radial distance ranges are limited to the channel portions crossing the reflector graphite. As for the central exposure tube, the simulated data of channels 4 and 8 are in satisfactory agreement with the available experimental ones. In

particular, the simulated flux profiles are of the same order of magnitude and accurately reproduce the patterns of the experimental datasets. These outcomes are encouraging for the subsequent activation reaction rate calculation starting from the simulated neutron flux in the graphite stack.

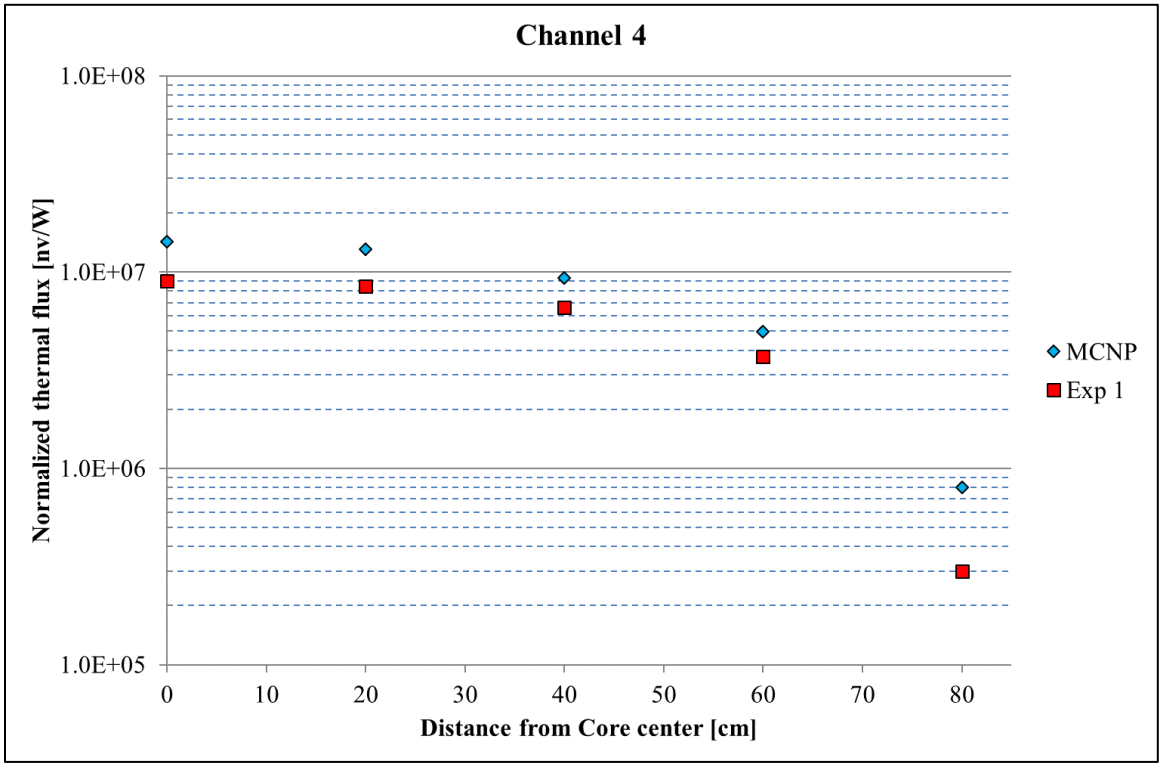

Figure 7 Normalized thermal flux in the exposure tube number 4 as a function of radial distance from the core. *MCNP* (blue diamond, this work), *Exp 1* (red square, experimental data from **[28]**). Experimental data are provided without uncertainty.

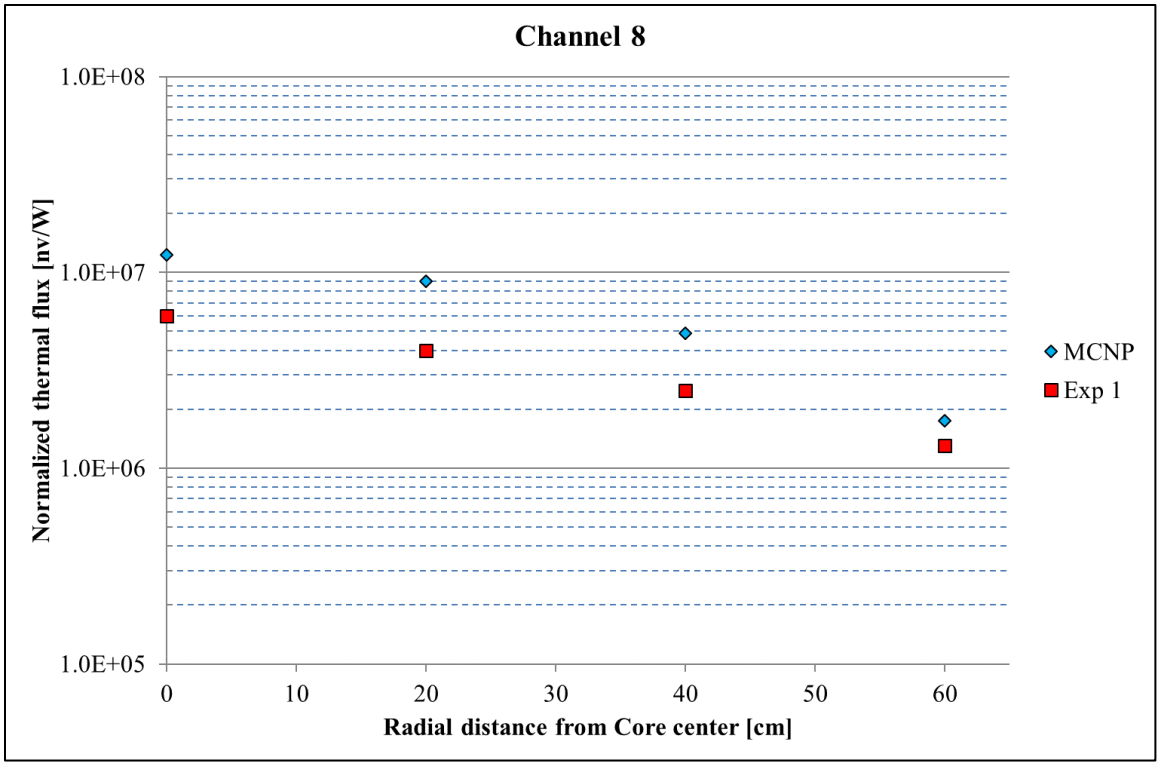

Figure 8 Normalized thermal flux in the exposure tube number 8 as a function of radial distance from the core. *MCNP* (blue diamond, this work), *Exp 1* (red square, experimental data from **[28]**). Experimental data are provided without uncertainty. MCNP error bars are within the marker size.

The reaction rates and the activity concentration distribution associated to ^{152}Eu and ^{154}Eu are calculated as elsewhere described [10] [11].

Comparison of gamma spectrometry and MCNP results

Concerning the irradiated graphite rods sampled and analyzed in this work, the comparison between their simulated activity concentrations and the experimental data are reported in Table 5 and

Table 6.

Table 5 Top rod: simulated ("*Sim.*") and experimental ("*Exp.*") ^{152,154}Eu activity concentration values and comparison ("*%Δ*") calculated as difference between simulated and experimental data.

	0 cm	**10 cm**	**20 cm**	**40 cm**	**68 cm**	

^{152}Eu [Bq g^{-1}]	189.5 ± 8.8	168.7 ± 7.4	135.8 ± 6.0	76.5 ± 3.4	30.5 ± 1.3	**Sim.**
	198.85 ± 0.98	185.50 ± 0.93	161.02 ± 0.82	100.15 ± 0.60	57.25 ± 0.40	**Exp.**
	-5%	-9%	-16%	-24%	-47%	**%Δ**
^{154}Eu [Bq g^{-1}]	3.32 ± 0.16	2.72 ± 0.13	2.10 ± 0.10	1.13 ± 0.05	0.44 ± 0.02	**Sim.**
	5.60 ± 0.10	4.82 ± 0.08	3.96 ± 0.08	2.23 ± 0.05	1.24 ± 0.04	**Exp.**
	-41%	-44%	-47%	-49%	-65%	**%Δ**

Table 6 Bottom rod: simulated ("*Sim.*") and experimental ("*Exp.*") ^{152,154}Eu activity concentration values and comparison ("*%Δ*") calculated as difference between simulated and experimental data.

	0 cm	**10 cm**	**20 cm**	**40 cm**	**68 cm**	
^{152}Eu [Bq g^{-1}]	223.5 ± 9.2	192.6 ± 7.9	151.7 ± 6.3	83.3 ± 3.5	32.7 ± 1.4	**Sim.**
	377.47 ± 1.70	353.35 ± 1.61	284.54 ± 1.35	164.45 ± 0.87	63.86 ± 0.42	**Exp.**
	-41%	-45%	-47%	-49%	-49%	**%Δ**
^{154}Eu [Bq g^{-1}]	3.99 ± 0.17	3.13 ± 0.13	2.36 ± 0.10	1.23 ± 0.05	0.48 ± 0.02	**Sim.**
	10.71 ± 0.14	9.13 ± 0.13	6.86 ± 0.11	3.71 ± 0.09	1.39 ± 0.04	**Exp.**
	-63%	-66%	-66%	-67%	-65%	**%Δ**

Given the already mentioned input data gaps and code implementation issues, satisfactory accordance between simulated and preliminary radiometric data has been proven, thus demonstrating the validity of the developed model [15]. In particular, the simulated activity concentration values are slightly underestimating the experimental ones, but are of the same order of magnitude and accurately reproduce their radial profile. The underestimate of the measured values is between -5% and -49% for ^{152}Eu and between -41% and -67% for ^{154}Eu. The latter radionuclide suffers of higher inaccuracy than ^{152}Eu, probably due to neutronic statistical issues, *i.e.*: less probable activation reactions on ^{153}Eu rather than on ^{151}Eu.

An increasing loss of accuracy is evidenced along the length of the graphite rods. This could be due to the lesser number of neutrons available, that worsen the statistics and enhances the impact of scarcely accurate input data. Furthermore, it can be evidenced that the model seems to be more accurate in the simulation of the top graphite rod rather than the bottom one. A possible explanation of the slight discrepancy between simulated and

experimental data could lay in some missing or misleading data about the operational history of the reactor and the exact composition, dimension and location of some components, such as shielding materials. As well, the activation precursors distribution has been considered uniform in the whole graphite stack, assuming the values of a previous elemental characterization on a virgin graphite sample [14]. Alteration of this parameter would more strongly affect the simulated activity concentration of the activation model, rather than the calculated neutron fluxes. Finally, there are no recorded information about possible configuration modifications.

Conclusions

This work presents the validation of a neutronic activation model on the basis of an experimental radiological characterization campaign. Several irradiated graphite samples have been collected and their gamma-emitting radionuclides content assessed by HPGe analyses. The developed MCNP model turned out to be satisfactorily accurate to simulate the neutron activation of L-54M nuclear research reactor structures and components. The discrepancy between simulated and experimental data could lay in some missing or inaccurate data about the operational history of the reactor or the exact composition, dimension and location of some components. In order to achieve a more accurate evaluation of activation precursors, further elemental analyses on virgin samples are foreseen for the next months. Prompt-gamma neutron activation analyses will be performed to quantify N and Cl precursors concentration and to verify other nuclides, Eu above all.

Taking into account all the given explanations and considerations, the herein developed neutronic model could be a promising and valid tool to support the radiological characterization of a nuclear facility undergoing decommissioning.

Some pure beta-emitting radionuclides (such as ^{3}H, ^{14}C, ^{36}Cl, $^{59,63}Ni$) will be considered and analyzed in the irradiated graphite samples collected during this work. These results will allow to definitely validate the developed neutronic model and to define a scaling

412 factor between easy and hard to measure radionuclides, both useful for subsequent
413 decommissioning activities.

414

415 Acknowledgements

416 This work was presented at the 2nd International Conference on Radioanalytical and
417 Nuclear Chemistry (RANC 2019) held in Budapest (H) on May 5th-10th 2019.

418 References

419

[1] W. E. Parkins, "Aqueous Homogeneous Type Research Reactors," North American Aviation. Atomics International Division., California, 1958.

[2] S. Terrani, "Reactor and nuclear facilities of the CeSNEF site: Safety report (Il reattore e gli impianti nucleari del CeSNEF - Rapporto di sicurezza)," Politecnico di Milano (Document written in Italian), Milano, 1961.

[3] E. Fermi, The Collected Papers of Enrico Fermi, vol. 2, E. Segre, Ed., Chicago, IL: University of Chicago Press, 1965.

[4] J. Buongiorno and D. Giuffrida, M.Sc. Thesis: Operations preliminary to L-54M reactor dismantling. (Operazioni preliminari allo smantellamento del reattore L-54 M), Milano: Politecnico di Milano (Document written in Italian), 1994-95.

[5] IAEA, "Decommissioning Strategies for Facilities Using Radioactive Material. Safety Reports Series No. 50," IAEA, Vienna, 2007.

[6] IAEA, "Advancing Implementation of Decommissioning and Environmental Remediation Programmes. Nuclear Energy Series No. NW-T-1.10. ISSN 1995–7807," IAEA, Vienna, 2016.

[7] OECD-NEA, "Costs of Decommissioning Nuclear Power Plants," OECD-NEA, Boulogne-Billancourt, 2016.

[8] N. R. C. (NUREG), "Consolidated Decommissioning Guidance, NUREG-1757, Vol.1," 2006.

[9] IAEA, "Transition from Operation to Decommissioning of Nuclear Installations, Technical Reports Series No. 420, ISSN 0074-1914," IAEA, Vienna, 2004.

[10] L. Castelli and D. Mapelli, M.Sc. Thesis: Decommissioning of L-54M CeSNEF reactor (Decommissioning del reattore L-54 M del CeSNEF), Milano: Politecnico di Milano (Document written in Italian), 2012-13.

[11] E. Mossini, L. Codispoti, M. Giola, L. Castelli, E. Macerata, A. Porta, F. Campi and M. Mariani, "Topsoil radiological characterisation of L-54M reactor surroundings

preliminary to decommissioning operations," *Journal of Environmental Radioactivity*, 2017.

[12] NUCLECO, "Final report of CeSNEF Pre-Decommissioning Activities (Rapporto finale per le attivita di pre-decommissioning del CeSNEF di Milano),," NUCLECO, Roma, 2016.

[13] A. Wickham, H.-J. Steinmetz, P. O'Sullivan and M. I. Ojovan, "Updating irradiated graphite disposal: Project GRAPA and the international decommissioning network," *Journal of Environmental Radioactivity*, pp. 34-40, 2017.

[14] G. Parma, et al., "MCNP model of L-54 M nuclear research reactor: development and preliminary verification," *J Radioanal Nucl Chem,* vol. 318, p. 2247–2255, 2018.

[15] E. Mossini, et al., "Monte Carlo integrated approach to radiological characterization for nuclear facilities decommissioning," *Radiat Eff Defect S,* vol. 173, pp. 772-783, 2018.

[16] T. Goorley, M. James, T. Booth, F. Brown, J. Bull and L. J. Cox, "Initial MCNP6 Release Overview," *Nuclear Technology*, pp. 298-315, 2012.

[17] IAEA, "Radiological Characterization of Shut Down Nuclear Reactors for Decommissioning Purposes. Technical Reports Series No. 389," IAEA, Vienna, 1998.

[18] R. Plukiene, A. Plukis, A. Puzas, V. Remeikis, G. Duskesas and D. Germanas, "Modeling of impurities activation in the RBMK reactor graphite using MCNPX," in *Joint international conference on supercomputing in nuclear applications and Monte Carlo*, Tokyo, 2010.

[19] ICRP, "The 2007 Recommendations of the International Commission on Radiological Protection. ICRP Pubblication 103, 2017 Ann. ICRP 37 (2-4)," ICRP, Ottawa, 2007.

[20] D.Lgs 230/95, *Legislative Decree of Government n. 230/95 and Subsequent Modifications and Additions (Decreto Legislativo del Governo 230/95 e Successive Modifiche ed Aggiunte - Attuazione delle direttive Euratom in materia di radiazioni ionizzanti),* Italy, 17 March 1995.

[21] ICRP, "Individual Monitoring for Internal Exposure of Workers. ICRP Publication 78, 1997, Ann ICRP 27 (3-4)," ICRP, Ottawa, 1997.

[22] UNI, "UNI 11665, Determination of gamma emitting radionuclides by high-resolution gamma spectrometry (in Italian: Determinazione di radionuclidi gamma emettitori mediante spettrometria gamma ad alta risoluzione)," UNI, Milano, 2017.

[23] ORTEC, "GammaVision A66-BW Software User's Manual, Version 7, revision H," ORTEC, 2013.

[24] CID Media GmbH, "GESPECOR Manual, Version 4.2," CID Media GmbH, Germany, 2007.

[25] International Organization for Standardization, ISO 11929:2010 Determination of the characteristic limits (decision threshold, detection limit and limits of the confidence interval) for measurements of ionizing radiation - Fundamentals and application, Geneva: International Organization for Standardization, 2010.

[26] D. Ancius, D. Ridikas, V. Remeikis, A. Plukis, R. Plukiene and M. Cometto, "Evaluation of the activity of irradiated graphite in the Ignalina Nuclear Power Plant RBMK-1500 reactor," *Nukleonika*, pp. 113-120, 2005.

[27] LOS ALAMOS NATIONAL LABORATORY, "MCNP: A General Montecarlo N-Particle Transport Code. Rep. LA-12625-M," Los Alamos, NM, 1993.

[28] Atomics International, *L-54 M Blueprints,* 1959.

[29] A. Hassid, M.Sc. Thesis: L-54M CeSNEF reactor. Plant, start-up, control, first measurements. (Il reattore L-54 del CeSNEF. Impianto, avviamento, controllo, prime misure.), Milano: Politecnico di Milano (Document written in Italian), 1958-59.

[30] M. Terrani, "M.Sc. Thesis: L-54M CeSNEF reactor. Measurement of neutron flux and determination of generated power. (Il reattore L-54 del CeSNEF. Misure di flussi neutronici e determinazione della potenza)," Politecnico di Milano (Document written in Italian), Milano, 1959-60.

[31] IAEA, "Decommissioning of Nuclear Power Plants and Research Reactors. Safety Standards Series No. WS-G-2.1," IAEA, Vienna, 1999.

[32] IAEA, "Decommissioning of Facilities. IAEA Safety Standards, No. GSR Part 6. ISSN 1020–525X," IAEA, Vienna, 2014.

[33] IAEA, "Selection of decommissioning strategies: Issues and factors. IAEA-TECDOC-1478," IAEA, Vienna, 2005.

[34] IAEA, "Strategy and Methodology for Radioactive Waste Characterization. IAEA-TECDOC-1537," IAEA, Vienna, 2007.

[35] IAEA, Status Of The Decommissioning Of Nuclear Facilities Around The World, Vienna: International Atomic Energy Agency, 2004.

420
421